Heliyon 10 (2024) e29164

Contents lists available at ScienceDirect

Heliyon

journal homepage: www.cell.com/heliyon

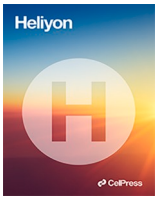

Research article

The potential molecular mechanism underlying gypenoside amelioration of atherosclerosis in ApoE$^{-/-}$ mice: A multi-omics investigation

Xing Ju [a,b,1], Yufeng Liu [c,1], Ying Wang [a,b], Guoyuan Sui [d], Yixin Ma [a,b], Huimin Cao [a,b], Yuan Cao [a,b], Jin Wu [a,b], Ying Du [a,b], Xue Leng [d], Lianqun Jia [b,*], Guanlin Yang [b,**]

[a] TCM Innovation Engineering Technology Center, Liaoning University of Traditional Chinese Medicine, Shenyang, 110847, China
[b] Key Laboratory of Ministry of Education for TCM Viscera-State Theory and Applications, Liaoning University of Traditional Chinese Medicine, Shenyang, 110847, China
[c] Center for Medical Research on Innovation and Translation, Guangzhou First People' S Hospital, Guangzhou, 510180, China
[d] School of Integrated Traditional Chinese and Western Medicine, Liaoning University of Traditional Chinese Medicine, Shenyang, 110847, China

ARTICLE INFO

Keywords:
Gypenosides
Arteriosclerosis
Metabolomics
Transcriptomics

ABSTRACT

Gypenosides (Gyp) are bioactive components of *Gynostemma pentaphyllum* that have a variety of pharmacological properties. Extracts of *G. pentaphyllum* have been found to be effective in the reduction of blood sugar and lipids and prevention of atherosclerosis. Here, the functions of Gyp and the mechanisms underlying their effects on atherosclerosis were investigated. Mice were allocated to three groups, namely, the control (C57BL/6), atherosclerosis model (ApoE$^{-/-}$ mice with high-fat diet), and Gyp-treated groups. Differentially expressed mRNAs, miRNAs, circRNA, and differential metabolites among the groups were analyzed. The results showed that "Fatty acid metabolism", "Fatty acid elongation", "Cytokine-cytokine receptor interaction", and "PI3K-Akt signaling pathway", amongst others, were involved in treatment process. Differentially expressed genes, including *Fabp1, Apoe, FADS1*, *ADH1, SYNPO2*, and *Lmod1*were also identified. Mmu-miR-30a and mmu-miR-30e showed reduced expression in atherosclerosis models but were increased following Gyp treatment, suggesting involvement in the effects of Gyp. In addition, chr5:150604177-150608440 were found to interact with mmu-miR-30a and mmu-miR-30e to regulate their abundance. In terms of metabolomics, Gyp may regulate biological processes involving PGD_2 and PGJ_2, potentially alleviating atherosclerosis. In conclusion, Gyp appeared to have complex effects on atherosclerosis, most of which were positive. These results support the use of Gyp in the treatment of atherosclerosis.

1. Introduction

Atherosclerosis results from dysfunctional lipid metabolism and contributes significantly to unstable coronary syndromes and

* Corresponding author.
** Corresponding author.
E-mail addresses: jlq-8@163.com (L. Jia), yang_guanlin@163.com (G. Yang).
[1] These authors contributed equally to this work.

https://doi.org/10.1016/j.heliyon.2024.e29164
Received 8 October 2023; Received in revised form 1 April 2024; Accepted 2 April 2024
Available online 10 April 2024

sudden cardiac death, even in young adults [1]. Since 2014, the incidence of cardiovascular disease caused by atherosclerosis has risen sharply in many countries, resulting in mortality rates second only to infectious diseases [2,3]. The pathogenesis of atherosclerosis resulting from dyslipidemia is complex. Several studies have found that lipid-induced endothelial cell injury and abnormal inflammatory responses are key factors in its development [4,5]. Endothelial cells act as the initial barrier in the protection of blood vessels. Atherosclerosis begins with damage to endothelial cells, leading to cellular dysfunction and, ultimately, infiltration by mononuclear cells and macrophages, the relocation of vascular smooth muscle cells to the intima, and phagocytosis of lipids to form foam cells [6]. At the same time, endothelial and inflammatory cells secrete various pro-inflammatory factors, leading to the development of atherosclerotic plaques [7].

Although long-term or short-term administration of statins can benefit the primary and secondary prevention of atherosclerotic cardiovascular disease, many patients are unable to reduce their cholesterol levels sufficiently [8]. While statins remain the first choice for the treatment of atherosclerosis, traditional Chinese medicine formulations based on Chinese herbal medicine have also been used in China and other Asian countries since the 1980s [9]. There are many clinical and experimental reports of the lipid-lowering efficacy of plants used in traditional Chinese medicines, including *Ligusticum chuanxiong* Hort., rhubarb, and *Alisma orientalis*, as well as hawthorn fruit, garlic, celery, and onion [9,10]. Although traditional Chinese medicine has been used for over 2000 years in China and many formulations have good curative effects on atherosclerotic diseases, there are still many difficulties in its use and acceptance. These are due to a lack of scientific basis evaluated by strict clinical trials, the complexity of its ingredients, and unclear pharmacological effects, which have hindered its wider application. Gypenosides (Gyp) are extracted from *Gynostemma pentaphyllum* and have

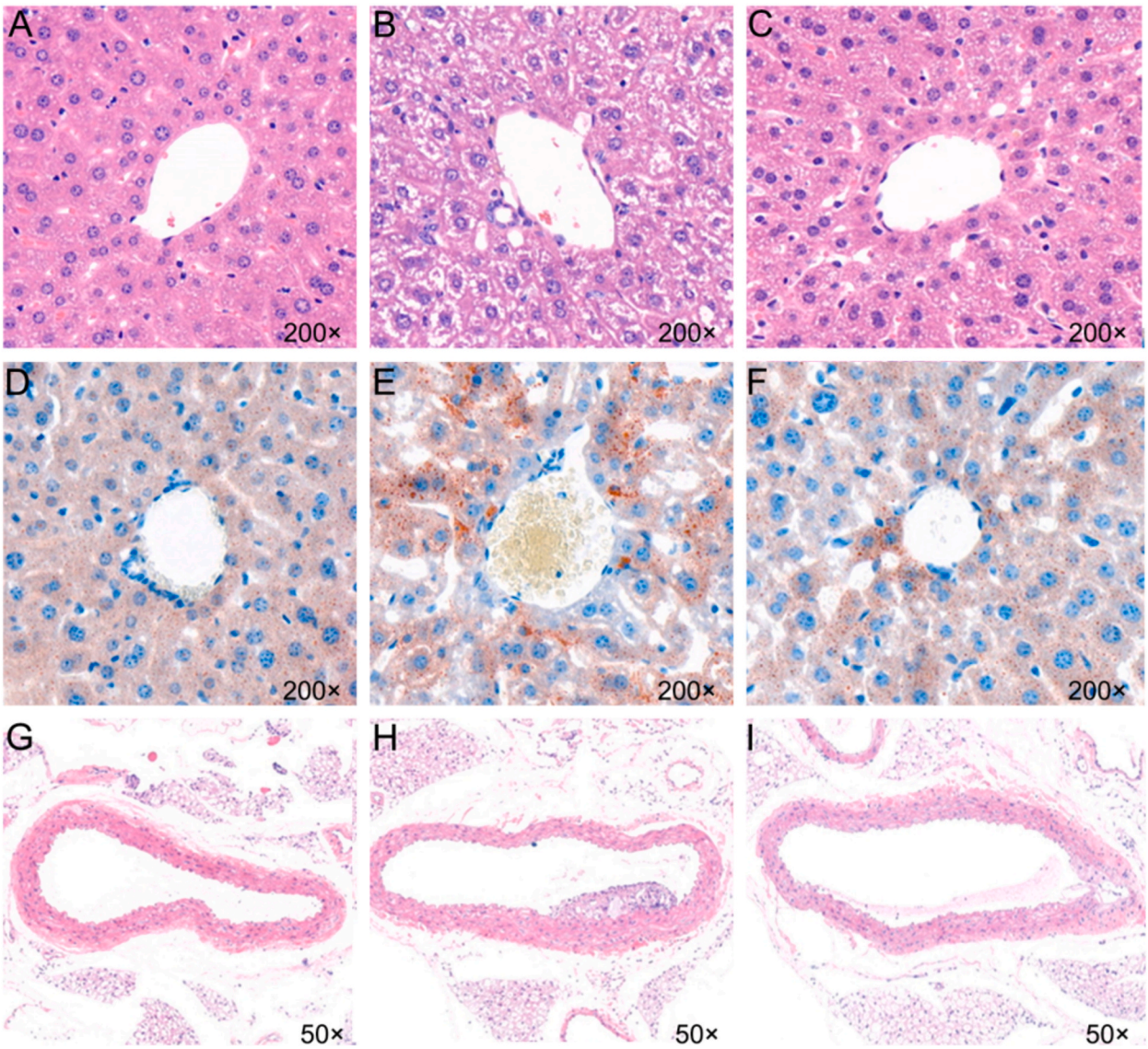

Fig. 1. Histological analysis of aorta and liver tissues.

been found to have a variety of pharmacological activities [11,12]. Ge et al. found that Gyp could protect cardiac muscle and improve its function in rat models of diabetic cardiomyopathy [13]. Moreover, Gyp was found to mitigate myocardial ischemia-reperfusion injury by alleviation of oxidative stress and mitochondrial damage [14]. Several studies have also shown that *G. pentaphyllum* extracts can lower blood lipid levels, prevent arteriosclerosis, reduce blood sugar, and modulate the immune response [15–18].

In this study, Gyp was used to treat atherosclerosis in apolipoprotein E knockout ($ApoE^{-/-}$) mice fed on high-fat diets. We hypothesized that Gyp could improve the symptoms of atherosclerosis through the modulation of molecular functions. Differentially expressed mRNAs, miRNAs, circRNAs, and differential metabolites among the control, model, and Gyp-treated groups were identified. The focus of the study was the action of Gyp and the mechanisms underlying its treatment of atherosclerosis.

2. Results

2.1. Changes in lipid deposition in the liver and atherosclerotic plaques following gypenoside treatment

Histological analyses were performed on liver and aorta samples to assess the success of the atherosclerotic model and the response to treatment. After staining, it was observed that the liver structure was normal in the control group, with characteristic arrangements of the hepatic cord and sinusoid in the center of the liver lobule. The hepatocytes appeared round, the cytoplasm was homogeneous and eosinophilic, and the nucleus was large and round (Fig. 1A). The structures of intima media, tunicae media, and adventitia in the aorta were normal. The intima was smooth with no evidence of fat spots or lines (Fig. 1G). In the $ApoE^{-/-}$ mice, the structure of the liver tissue appeared disordered, with narrowing of the hepatic sinusoid. The hepatocytes were enlarged with loose cytoplasm, and some binuclear hepatocytes could be seen (Fig. 1B).The intimal bulge of the artery was thickened due to both lipid deposition and plaque formation, among which foam cells and cholesterol crystals could be observed (Fig. 1H). In the Gyp group, the structures of both the liver and arteries resembled those of the normal group, and no lipid deposition or plaque formation was visible (Fig. 1C and I). On Oil Red O staining, no cell swelling or steatosis was visible in hepatocytes from the normal group (Fig. 1D), while those from $ApoE^{-/-}$ mice were obviously steatotic, containing fat droplets of different sizes (Fig. 1E). In contrast, the Gyp group showed markedly reduced numbers of lipid droplets in the liver tissue, closely resembling the tissues of the normal group (Fig. 1F).

2.2. Blood biochemical indices

The TC, TG, LDL, and HDL levels were found to be 42.64 ± 2.37, 0.88 ± 0.05, 16.26 ± 2.18, and 2.44 ± 0.23 mmol/l, respectively, in mice from the model group. Of these, the TG, TC, and LDL levels were markedly raised in the model group in comparison with the control and Gyp-treated groups ($P < 0.05$), whereas the HDL levels did not alter significantly ($P > 0.05$, Fig. 2). Levels of both TC and LDL were elevated in the Gyp group relative to the controls. These results indicated that Gyp treatment reduced the levels of blood lipids in atherosclerotic mice.

2.3. DEGs in the different groups

RNA from the three groups was sequenced, with three biological replicates per group (termed 1, 2, and 3). Totals of 18,563,894, 11,364,402, and 15,067,846 aligned reads with Q30 > 92% bases were obtained for the control, model, and Gyp groups, respectively, after the exclusion of low-quality reads (Q-value <20), adaptor sequences, and reads with >10% of ambiguous "N" bases. The average GC content over all samples was approximately 48%. Comparable results were obtained for the biological replicates (Table 1).

Overall, 1071, 200, and 750 DEGs were identified between the Model vs Control, Gyp vs Model, and Gyp vs Control groups, respectively (Fig. 3A). Of these, 22, including *Gpnmb*, *Cyp1a2*, *Bdh1*, *Fabp1*, *Apoe*, and *Naip6*, were found to be common (Fig. 3B and C). Many of these genes are related to fatty metabolism and significant enrichment was observed in lipid-associated GO biological processes, including "lipid metabolic process" (GO:0006629), "fatty acid metabolic process" (GO:0006631), and "lipid biosynthetic

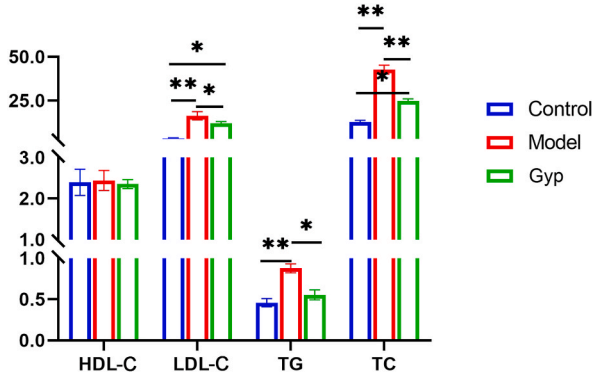

Fig. 2. Blood biochemical indices.

Table 1
DEGs in the different groups.

name	Raw Reads	Adaptor Trimmed Reads (≥15 nt)	Aligned Reads	sample	Q30
Control1	9,961,024	9,452,707	6,386,425	Model1	97.06%
Control2	8,454,994	7,989,006	5,089,208	Model2	96.47%
Control3	10,708,789	10,414,824	7,088,261	Model3	95.53%
Gps1	12,442,082	11,332,193	3,644,836	Gps1	95.62%
Gps2	12,634,830	12,046,877	5,259,218	Gps2	95.96%
Gps3	10,795,155	10,344,985	6,163,792	Gps3	97.07%
Model1	9,404,303	8,744,234	4,363,340	Control1	97.40%
Model2	12,511,465	11,074,881	3,910,304	Control2	97.31%
Model3	11,989,285	10,455,061	3,090,758	Control3	96.86%

process" (GO:0008610). Many DEGs were also enriched in lipid metabolism-associated KEGG pathways, such as "Fatty acid metabolism" (mmu01212), "Fatty acid elongation" (mmu00062), "Fatty acid degradation" (mmu00071), and "Cytokine-cytokine receptor interaction" (mmu04060). Enrichment was also observed in various signaling pathways "Cytokine-cytokine receptor interaction" (mmu04060), "NOD-like receptor signaling pathway" (mmu04621), and "PI3K-Akt signaling pathway" (mmu04151). The enriched lipid-associated DEGs included *Fabp, Apoe, Acot, FADS2, ADH1, ALDH,* and *SREBF* (Fig. 3D) with upregulation in the model group but with reduced expression following Gyp treatment. In contrast, the two genes were minimally expressed in the controls (Fig. 3E).

2.4. Differentially expressed miRNA (DEmiRNA) and target genes

A total of 655 miRNAs were found over all samples, of which 72 were differentially expressed (Fig. 4A and B). The five most abundantly expressed were mmu-miR-143-3p, mmu-miR-30a-3p, mmu-miR-30e-3p, mmu-miR-novel-chrM_43955, and mmu-miR-182-5p. Eighteen of the DEmiRNAs were found to have the most target genes (Table 2). Of these 18 miRNAs, six were observed to be upregulated, including mmu-miR-30a-3p, mmu-miR-30e-3p, mmu-miR-182-5p, mmu-miR-200a-5p, mmu-miR-200b-3p, and mmu-miR-200a-3p, suggesting their involvement in Gyp treatment. The levels of these miRNAs are shown in Fig. 4C.

Following the prediction of the target genes, several DEGs were found to be regulated by miRNAs, for example, *SYNPO2* was predicted to be targeted by both mmu-miR-30a-3p and mmu-miR-30e-3p, while *LMOD1* was targeted by mmu-miR-200a-3p. Other DEGs, such as *Abca1, Spon1*, and *Myo5a*, were also predicted to be targeted by DEmiRNAs.

2.5. Identification and expression of circRNAs

Overall, 2878 circRNAs were found in the three groups, of which 36 circRNAs were differentially expressed (Fig. 5A). The

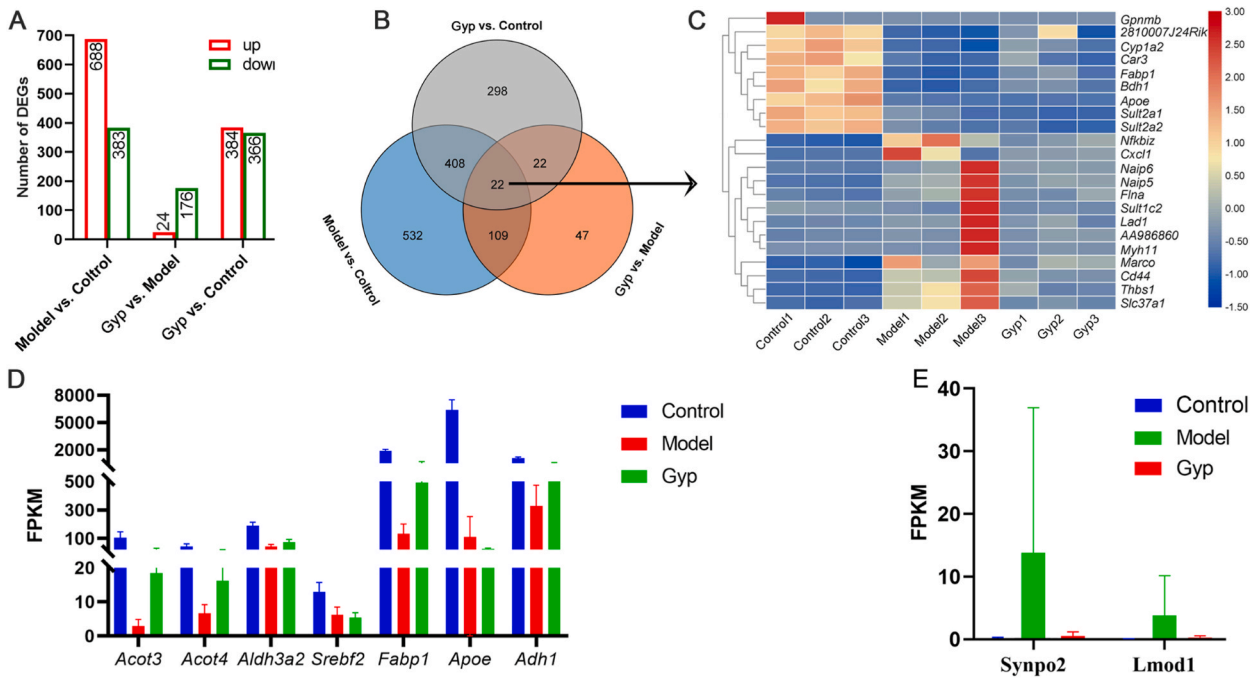

Fig. 3. Differentially expressed genes in the different groups.

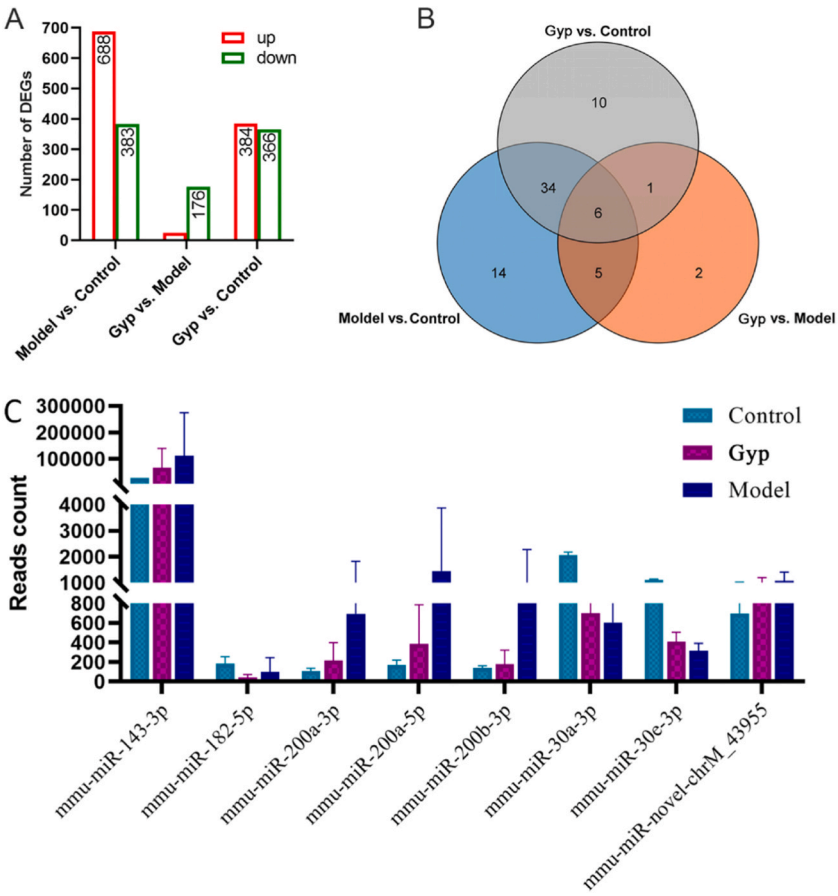

Fig. 4. Differentially expressed miRNA s(DEmiRNA) and their target genes.

Table 2
Information on miRNAs.

miRNA	Target genes number
mmu-miR-30a-3p	89
mmu-miR-182-5p	228
mmu-miR-1964-3p	73
mmu-miR-200a-3p	178
mmu-miR-200a-5p	68
mmu-miR-200b-3p	88
mmu-miR-200c-3p	92
mmu-miR-429-3p	97
mmu-miR-30e-3p	94
mmu-miR-1843a-3p	29
mmu-let-7c-1-3p	181
mmu-miR-1a-3p	159
mmu-miR-218-5p	215
mmu-miR-712-5p	184
mmu-miR-3081-3p	106
mmu-miR-871-3p	370
mmu-miR-881-3p	208
mmu-miR-204-5p	257

differentially expressed circRNAs were further evaluated in terms of their fold changes (FCs), statistical values, and raw signal intensities to reduce the list and improve the accuracy of identification. This led to the selection of seven circRNAs for further analysis. The expression levels of these seven circRNAs are shown in Fig. 5B. Differential expression of chr11:20725685–20727639-, chr1:139593754-139628309-, chrY:90793079–90793680+, and chr5:150604177-150608440 was seen between the control and model groups, as well as between the model and Gyp groups, but not between the control and Gyp groups. The miRNAs targeting these

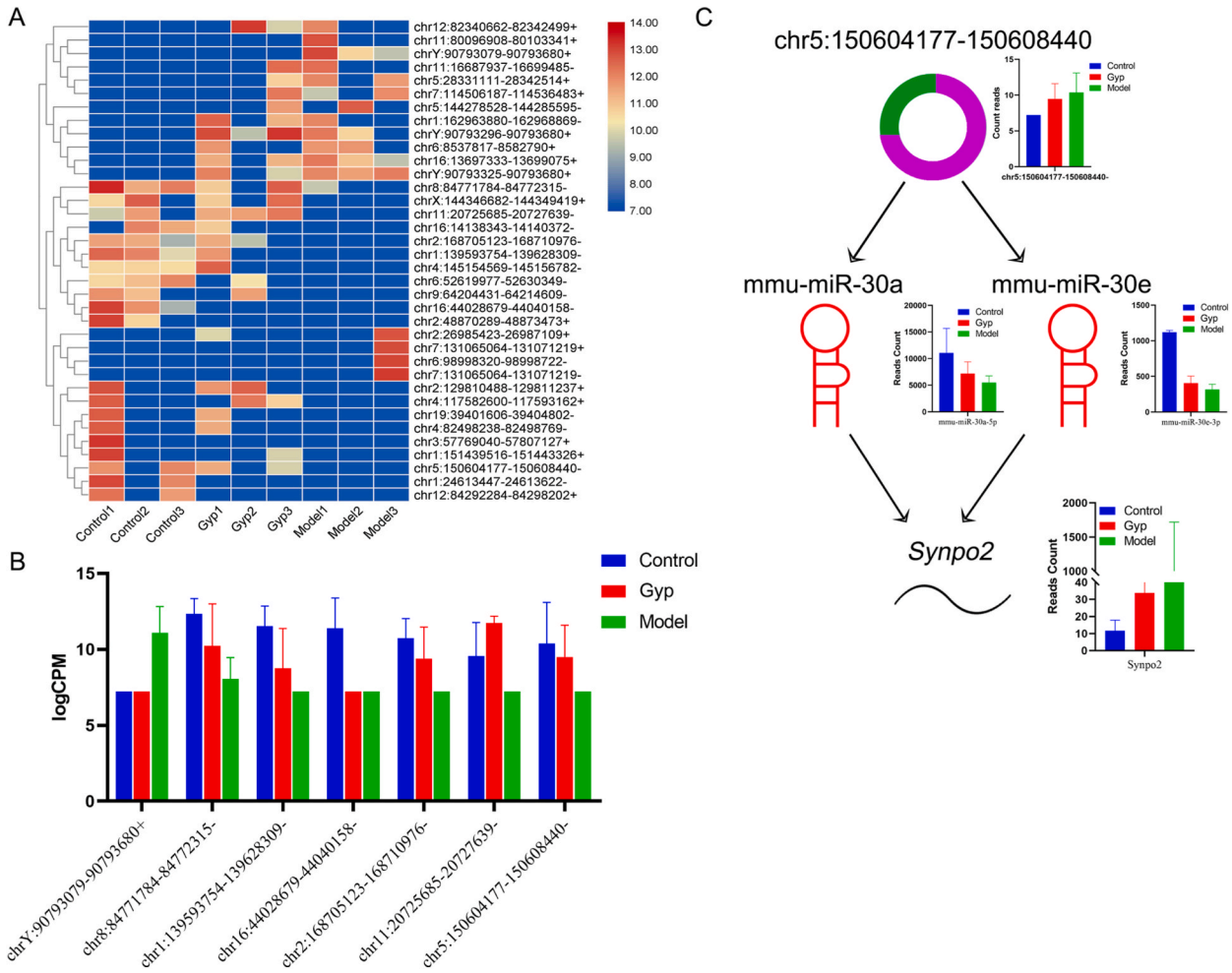

Fig. 5. Identification and expression of circRNAs.

circRNAs were then predicted to determine their functions. It was predicted that the identified miRNAs mmu-miR-30a and mmu-miR-30e were both targeted by chr5:150604177-150608440-. Fig. 5C illustrates the expression and interactions between chr5:150604177-150608440-, mmu-miR-30, and the *Synpo2* gene. Levels of chr5:150604177-150608440- were negatively associated with those of mmu-miR-30, but positively associated with *Synpo2*.

2.6. *Differential metabolites*

PCA was used to examine the consistency between the biological replicates in all samples. This showed a distinct differentiation between the control and model groups while the model and Gyp groups were indistinguishable, indicating similar metabolic profiles in these two groups (Fig. 6A–C). A total of 122 differential metabolites were identified. The heatmap of these differential metabolites confirmed the similarity between the model and Gyp groups (Fig. 6D). However, despite the similarity between the metabolic profiles of the model and Gyp groups, some differences were apparent. As shown in the Venn diagram (Fig. 6E), seven metabolites were shared between the control vs model and Gyp vs model groups. Specifically, PGD_2, PGJ_2, δ-Valerolactam, and dihydroactinidiolide were upregulated in the model group while indole-2-carboxylic acid, N-feruloyl putrescine, and ergothioneine were downregulated. It is thus possible that these metabolites may be involved in atherosclerosis development.

qRT-PCR verification.

The levels of *Fabp1, Apoe, Fads1, Adh1, and Synpo2* were measured and found to be consistent with the results of the transcriptomic analysis (Fig. 7A). It was also found that mmu-miR-30a expression in the control group was markedly higher. The levels of mmu-miR-30e-3p were essentially similar in all groups (Fig. 7B). The candidate circRNA chr5:150604177-150608440- showed highest expression in the control but lowest in the model group (Fig. 7C).

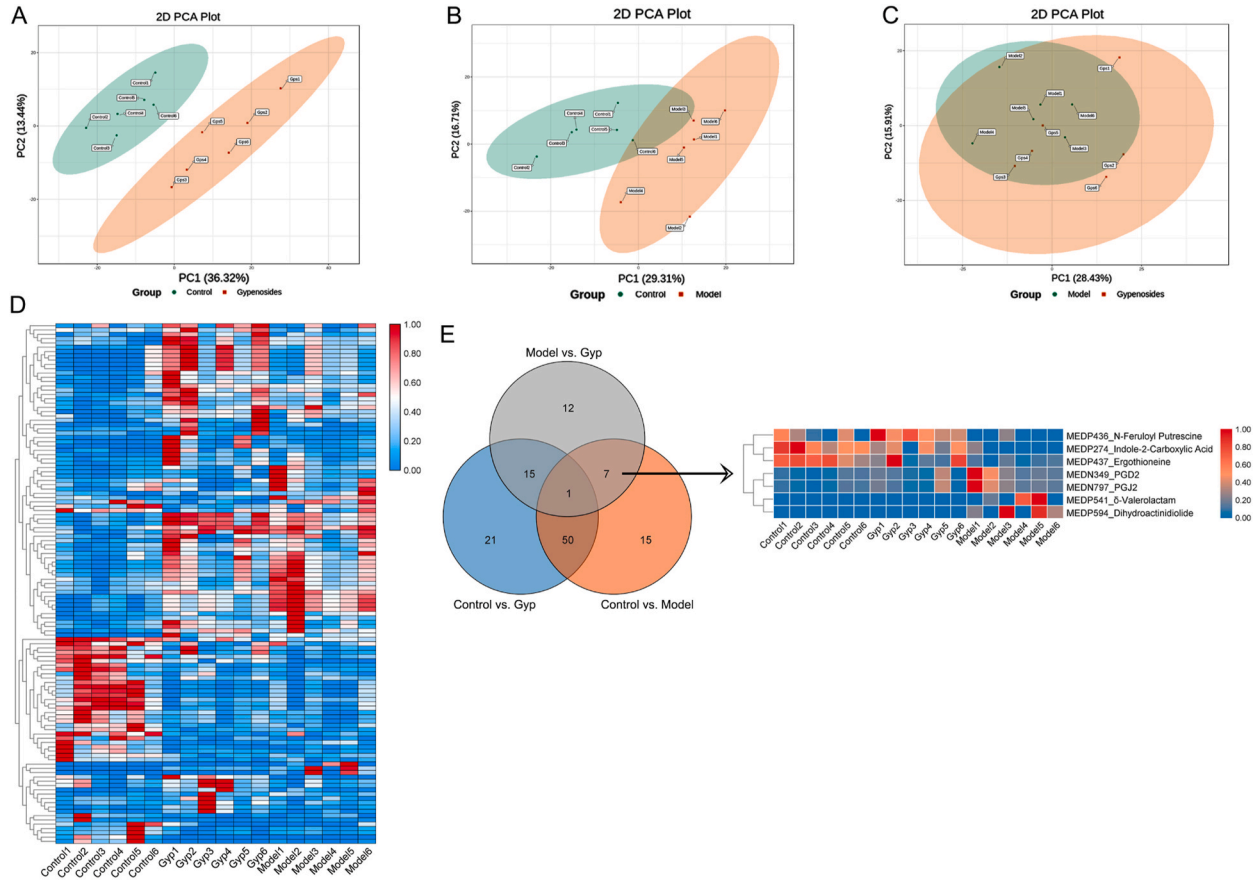

Fig. 6. Expression of differential metabolites.

3. Discussion

Here, the genome-wide mRNA, miRNA, and circRNA expression profiles, together with differential metabolites, were investigated in normal and ApoE$^{-/-}$ mice fed on high-fat diets using high-throughput sequencing and LC/MS. The successful construction of the atherosclerotic model was confirmed by microscopy and blood lipid analysis0. The mitochondria were greatly affected by the high-fat diet and LDL, TG, and TC levels were markedly increased in the atherosclerotic model mice relative to the controls. However, the blood lipid levels were significantly lowered after Gyp treatment, although they did not return to the control levels. The analysis of DEG functions showed enrichment in pathways associated with "Fatty acid metabolism" (mmu01212), "Fatty acid elongation" (mmu00062), "Fatty acid degradation" (mmu00071), "Cytokine-cytokine receptor interaction" (mmu04060). Furthermore, the expression of *Bdh1, Fabp1,* and *Apoe* was markedly higher in the control mice compared with the models. ApoE$^{-/-}$ mice have symptoms similar to those seen in human atherosclerosis, including hyperlipidemia resulting from reduced clearance of lipoproteins [19]. Therefore, it is not difficult to understand the decrease in ApoE in atherosclerosis models. FABPs are cytoplasmic lipid transporters implicated in atherosclerosis progression [20] and appear to be associated with inflammation, both chronic and low-grade. FABPs have been proposed as potential targets for atherosclerosis treatment [21]. *Fabp1* was observed to be downregulated in the model mice but increased following Gyp treatment, suggesting that Gyp was involved in fatty acid degradation. A similar expression trend was observed for *Bdh1*.

It was found that both *Synpo2* and *Lmod1* were upregulated in the model and Gyp groups. An earlier study reported dysregulation of various genes (*LMOD1, SYNPO2, PLIN2,* and *PPBP*) in atherosclerosis [22]. Of note, a *SYNPO2* variant was observed in the intronic region of *USP53* in the Biobank of Karolinska Endarterectomy study [23]. High levels of USP53 are seen in cardiac muscle and are associated with Cantu syndrome [24]. Here, it was found that *Synpo2* was targeted by both mmu-miR-30a and mmu-miR-30e with a negative association observed between *Synpo2* and mmu-miR-30. Overexpression of miR-30c in *ApoE*$^{-/-}$ mice has been found to mitigate atherosclerosis [25] and it has also been reported to reduce hyperlipidemia [25]. The present study observed lower levels of mmu-miR-30a and mmu-miR-30e in the model mice, confirming earlier findings [26], which were increased after Gyp treatment suggesting their potential involvement in Gyp action. Among the seven candidate circRNAs, chr5:150604177-150608440 interacted with mmu-miR-30a and mmu-miR-30e to regulate their levels. It is well known that circRNAs sponge miRNAs to modulate transcription [27–29] and chr5:150604177–150608440 may thus function in this manner. The present study showed that

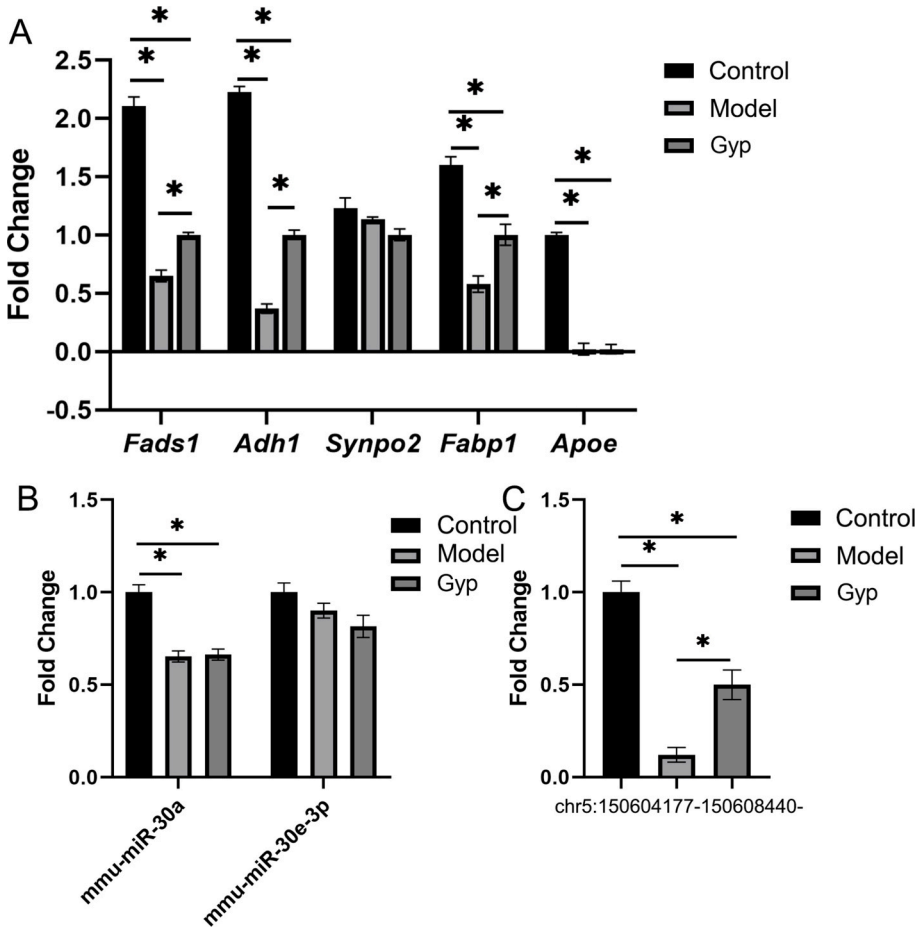

Fig. 7. qRT-PCR verification.

chr5:150604177-150608440 was negatively correlated with both mmu-miR-30a and mmu-miR-30e but positively associated with their target genes (such as *Synpo2*).

The metabolomics analysis identified several metabolites associated with the effects of Gyp in atherosclerosis. PGD_2, PGJ_2, δ-valerolactam, dihydroactinidiolide, indole-2-carboxylic acid, N-feruloyl putrescine, and ergothioneine were identified as seven candidate metabolites potentially involved in atherosclerosis development. Guan et al. reported that PGD_2 and PGJ_2 upregulate MMP-1 expression [30]. The enzyme PGD is responsible for the conversion of PGH_2 during arachidonic acid metabolism. PGD_2 is then metabolized nonenzymatically to the PGJ_2 series of metabolites, including PGJ_2, delta^{12}-PGJ_2, and 15-deoxy-delta^{12,14}-PGJ_2 (15d-PGJ_2) [31]. PGD_2 and PGJ_2 contribute to anti-inflammatory effects of L-PGDS in human atherosclerotic plaques [32]. PGD and its associated enzymes are implicated in the development of conditioned heart hypertrophy, thrombosis, and atherosclerosis [33–35]. The atherosclerotic model mice showed high levels of PGD_2 and PGJ_2, which were reduced by Gyp. The findings suggest that Gyp may modulate biological processes involving PGD_2 and PGJ_2, potentially alleviating atherosclerosis.

In conclusion, it appears that Gyp has complex effects on atherosclerosis, most of which were positive, supporting the use of Gyp in the treatment of atherosclerosis.

Systems genetics has opened up directions for the investigation of complex diseases, although there are still many challenges in its practical application. First, the accurate identification and measurement of the relationships between genetic variations and disease remain key issues. Currently used tests may not capture the full range of genetic variation, leading to inaccuracies in study results. Second, the genetic basis of complex diseases often involves interactions between multiple genes and the environment. A further issue is the application of laboratory findings to clinical practice. However, despite these challenges, systems genetics still holds great potential. As technology continues to advance, it is hoped to develop more accurate and comprehensive research methods. For example, the use of AI and analysis of big data allows in-depth investigation of the links between genetic variants and disease, together with the development of personalized diagnostics and treatments.

Future research using systems genetics will require interdisciplinary cooperation, allowing the combination of knowledge from multiple fields, such as biology, medicine, mathematics, and computer science. Through such collaboration, it is hoped to break through the bottlenecks of current research and provide more effective strategies for the treatment and management of complex

diseases.

4. Conclusion

Gyp treatment significantly reduced the levels of both TC and LDL, suggesting its potential for alleviating atherosclerosis. Pathways associated with "Fatty acid metabolism" (mmu01212), "Fatty acid elongation" (mmu00062), "Cytokine-cytokine receptor interaction" (mmu04060), and "PI3K-Akt signaling pathway" (mmu04151) were found to be enriched in the Gyp treatment process. The candidate DEGs identified included *Fabp, Apoe, Fads2*, *Adh1, Synpo2,* and *Lmod1*. In addition, miRNAs, including mmu-miR-30a and mmu-miR-30e, were found to be involved by modulating the levels of DEGs. These two miRNAs were targeted by chr5:150604177-150608440-. The metabolomics analysis indicated that Gyp may regulate biological processes involving PGD_2 and PGJ_2. In conclusion, the effects of Gyp on atherosclerosis appear complex, inducing many positive changes, and support the use of Gyp for the treatment of atherosclerosis.

5. Materials and methods

5.1. Ethics statement

This study was carried out in strict accordance with the recommendations in the Guide for the Care and Use of Laboratory Animals of the National Institutes of Health (Publication No. 85–23, revised 1996). The protocol was approved by the Institutional Animal Care and Use Committee of Liaoning University of Traditional Chinese Medicine. The experimental animals used in this study were obtained from Liaoning Changsheng Biotechnology Co., LTD (Permit Number SCXK [Liao] 2020-0001).

5.2. Experimental animals

The experimental animals were six $ApoE^{-/-}$ mice (C57BL/6 genetic background, eight weeks old, male) and three wild-type (WT) C57BL/6 mice. After acclimatization for one week, the six $ApoE^{-/-}$ mice were randomly allocated to two groups, namely, the model and Gyp-treated groups (each $n = 3$). The mice were then freely fed a high-fat diet with 20% fat and 1.5% cholesterol. The control mice were maintained on a normal diet. Mice in the Gyp-treated group received daily intraperitoneal injections of 25 mg/kg body weight (bw) Gyp for eight weeks while vehicle was similarly administered to the remaining mice.

Measurement of total cholesterol (TC), low-density lipoprotein (LDL), high-density lipoprotein (HDL), and triglycerides (TG)

Blood samples were collected by retro-orbital sinus after anesthesia with pentobarbital sodium (50 mg/kg, IP). ELISA kits were used to measure the TC, LDL, HDL, and TG levels, in accordance with the provided instructions.

5.3. Liver tissue preparation and histological staining

Mice were anesthetized as above and the livers and aortas were harvested and immediately washed in PBS. The tissues were fixed in 10% neutral buffered formalin for 48 h before paraffin embedding and sectioning (5 μm sections). The sections were then stained with H&E, as previously described [36,37].

5.4. Extraction and sequencing of liver RNA

RNA was extracted from liver tissue using TRIzol (Invitrogen, Waltham, MA, USA) and its quality was assessed on an Agilent 2100 Bioanalyzer (Agilent Technologies, Santa Clara, CA, USA) The RNA was then purified using a RNeasy mini kit (Qiagen, Hilden, Germany). Ribosomal RNA (rRNA) was removed using a Ribo-Zero Magnetic kit (Epicentre, Madison, WI, USA) and RNase R (Epicentre) was used for linear RNA before constructing the RNA-seq libraries. Following the removal of the rRNA and linear RNA, the samples were fragmented and reverse-transcribed to cDNA using random hexamer primers. After construction using a VAHTSTM Total RNA-seq (H/M/R) Library Prep Kit, the libraries were sequenced on a HiSeq 4000 Illumina system (San Diego, CA, USA) using a 150-bp paired-end run.

5.5. Analysis of sequencing data

Quality control was performed using FastQC (V2.1), followed by alignment of the clean reads to the reference genome using STAR software. Differentially expressed genes (DEGs) were identified using the R package DESeq2 (version 1.24.0) [38], using padj <0.05 with the negative binomial distribution test and $|\log2FC| \geq 1$. Genes with $\log_2FC > 1$ and $\log_2FC < -1$ were defined as up- and down-regulated, respectively. The R heatmap package (version 1.0.10) was used for hierarchical clustering of DEGs according to the expression. GO and KEGG enrichment of the DEGs was then examined according to phenotype [39]. Significant ($p < 0.05$) KEGG pathways and GO biological processes (BP) were then determined. The circos figure was constructed using Circos software [40]. The junctions with unmapped reads were identified using a back-splice algorithm. The expression of circRNAs was normalized according to the transcripts per million (TPM) as Normalized expression level = (readCount × 1,000,000)/libsize (libsize is the sum of circRNA read count) [41]. The Benjamini and Hochberg approach was used for the adjustment of p-values to control the false discovery rate. CircRNAs with adjusted p-values <0.05 were considered differentially expressed.

5.6. Sample preparation and metabolome analyses

Liver tissues for metabolomics were prepared following previously described protocols [42,43]. Specifically, the tissue was homogenized using a homogenizer (Huaheng, Chengdu, China) and 1 ml of extraction liquid (1:1 [v/v] ratio of methanol and acetonitrile) was added for metabolite extraction. One hundred and 50 μL of water were then added and the material was vortexed for 30 s and ultrasonicated for 5 min. This process was repeated three times, followed by incubation for 1 h at −20 °C for protein precipitation. The material was centrifuged (12,000 rpm, 15 min, 4 °C) and vacuum-dried. The dried material was then resuspended in 200 μl of extraction liquid (1:1 ratio [v/v] of acetonitrile and water), followed by vortexing (30 s), sonication (10 min), and centrifugation (12, 000 rpm, 15 min, 4 °C). The supernatant was transferred to a 2 ml LC/MS glass vial and analyzed by UHPLC-Q-TOF-MS. Details of the separation and the parameters used are provided in Table S1.

5.7. qRT-PCR

The expression of genes of interest was evaluated by qRT-PCR on an Applied Biosystems 7900 Sequence Detection System.

5.8. Statistical analysis

Data were analyzed using GraphPad Prism (vision 9.0). Continuous data are presented as mean ± standard deviation. Behavioral data were analyzed using repeated measures ANOVA (RM ANOVA) or one-way ANOVA where appropriate with Tukey–Kramer post hoc tests. *P*-values <0.05 were considered statistically significant.

Ethics approval and consent to participate

The protocol was approved by the Institutional Animal Care and Use Committee of Liaoning University of Traditional Chinese Medicine(Approval number: 21000092017068).

Availability of data and materials

All data generated or analyzed during this study are included in this published article.

Funding

This study was supported by Ministry of Education key laboratory open fund(zyzx2003); National Natural Science Foundation of China(82104552,82074145,81974548,82305061)

CRediT authorship contribution statement

Xing Ju: Writing – original draft, Data curation, Conceptualization. **Yufeng Liu:** Writing – original draft, Data curation, Conceptualization. **Ying Wang:** Formal analysis. **Guoyuan Sui:** Formal analysis. **Yixin Ma:** Methodology, Investigation. **Huimin Cao:** Methodology, Investigation. **Yuan Cao:** Methodology, Investigation. **Jin Wu:** Data curation. **Ying Du:** Investigation. **Xue Leng:** Formal analysis. **Lianqun Jia:** Writing – review & editing. **Guanlin Yang:** Writing – review & editing.

Declaration of competing interest

The authors declare that they have no known competing financial interests or personal relationships that could have appeared to influence the work reported in this paper.

Appendix A. Supplementary data

Supplementary data to this article can be found online at https://doi.org/10.1016/j.heliyon.2024.e29164.

References

[1] A.K. Pillay, D.P. Naidoo, Atherosclerotic disease is the predominant aetiology of acute coronary syndrome in young adults, Cardiovascular journal of Africa 29 (1) (2018) 36–42, https://doi.org/10.5830/CVJA-2017-035.

[2] Salim S. Virani, A. Alonso, J. Benjamin Emelia, S. Bittencourt Marcio, W. Callaway Clifton, P. Carson April, et al., Heart disease and stroke statistics—2020 update: a report from the American heart association, Circulation 141 (9) (2020) e139–e596, https://doi.org/10.1161/CIR.0000000000000757.

[3] D. Zhao, J. Liu, M. Wang, X. Zhang, M. Zhou, Epidemiology of cardiovascular disease in China: current features and implications, Nat. Rev. Cardiol. 16 (4) (2019) 203–212, https://doi.org/10.1038/s41569-018-0119-4.

[4] A. Zmysłowski, A. Szterk, Current knowledge on the mechanism of atherosclerosis and pro-atherosclerotic properties of oxysterols, Lipids Health Dis. 16 (1) (2017) 188, https://doi.org/10.1186/s12944-017-0579-2.

[5] M. Rafieian-Kopaei, M. Setorki, M. Doudi, A. Baradaran, H. Nasri, Atherosclerosis: process, indicators, risk factors and new hopes, Int. J. Prev. Med. 5 (8) (2014) 927–946.

[6] K.J. Moore, F.J. Sheedy, E.A. Fisher, Macrophages in atherosclerosis: a dynamic balance, Nat. Rev. Immunol. 13 (10) (2013) 709–721, https://doi.org/10.1038/nri3520.

[7] M.Y. Wu, C.J. Li, M.F. Hou, P.Y. Chu, New insights into the role of inflammation in the pathogenesis of atherosclerosis, Int. J. Mol. Sci. 18 (10) (2017), https://doi.org/10.3390/ijms18102034.

[8] D.G. Karalis, B. Victor, L. Ahedor, L. Liu, Use of lipid-lowering medications and the likelihood of achieving optimal LDL-cholesterol goals in coronary artery disease patients, Cholesterol 2012 (2012) 861924, https://doi.org/10.1155/2012/861924.

[9] C. Wang, M. Niimi, T. Watanabe, Y. Wang, J. Liang, J. Fan, Treatment of atherosclerosis by traditional Chinese medicine: questions and quandaries, Atherosclerosis 277 (2018) 136–144, https://doi.org/10.1016/j.atherosclerosis.2018.08.039.

[10] Z. Lu, W. Kou, B. Du, Y. Wu, S. Zhao, O.A. Brusco, et al., Effect of Xuezhikang, an extract from red yeast Chinese rice, on coronary events in a Chinese population with previous myocardial infarction, Am. J. Cardiol. 101 (12) (2008) 1689–1693, https://doi.org/10.1016/j.amjcard.2008.02.056.

[11] S. Megalli, F. Aktan, N.M. Davies, B.D. Roufogalis, Phytopreventative anti-hyperlipidemic effects of Gynostemma pentaphyllum in rats, J Pharm Pharm Sci 8 (3) (2005) 507–515.

[12] K.W. Lu, J.C. Chen, T.Y. Lai, J.S. Yang, S.W. Weng, Y.S. Ma, et al., Gypenosides suppress growth of human oral cancer SAS cells in vitro and in a murine xenograft model: the role of apoptosis mediated by caspase-dependent and caspase-independent pathways, Integr. Cancer Ther. 11 (2) (2012) 129–140, https://doi.org/10.1177/1534735411403306.

[13] M. Ge, S. Ma, L. Tao, S. Guan, The effect of gypenosides on cardiac function and expression of cytoskeletal genes of myocardium in diabetic cardiomyopathy rats, Am. J. Chin. Med. 37 (6) (2009) 1059–1068, https://doi.org/10.1142/s0192415x09007491.

[14] H. Yu, H. Zhang, W. Zhao, L. Guo, X. Li, Y. Li, et al., Gypenoside protects against myocardial ischemia-reperfusion injury by inhibiting cardiomyocytes apoptosis via inhibition of CHOP pathway and activation of PI3K/Akt pathway in Vivo and in vitro, Cell. Physiol. Biochem. 39 (1) (2016) 123–136, https://doi.org/10.1159/000445611.

[15] S.-Q. Dong, Q.-P. Zhang, J.-X. Zhu, M. Chen, C.-F. Li, Q. Liu, et al., Gypenosides reverses depressive behavior via inhibiting hippocampal neuroinflammation, Biomed. Pharmacother. 106 (2018) 1153–1160, https://doi.org/10.1016/j.biopha.2018.07.040.

[16] Y. Lu, Y. Du, L. Qin, D. Wu, W. Wang, L. Ling, et al., Gypenosides altered hepatic bile acids homeostasis in mice treated with high fat diet, Evid Based Complement Alternat Med 2018 (2018).

[17] Y. Lu, Y. Du, L. Qin, D. Wu, W. Wang, L. Ling, et al., Gypenosides altered hepatic bile acids homeostasis in mice treated with high fat diet, Evid Based Complement Alternat Med 2018 (2018) 8098059, https://doi.org/10.1155/2018/8098059.

[18] J. Wang, T.K.Q. Ha, Y.P. Shi, W.K. Oh, J.L. Yang, Hypoglycemic triterpenes from Gynostemma pentaphyllum, Phytochemistry 155 (2018) 171–181, https://doi.org/10.1016/j.phytochem.2018.08.008.

[19] K.-L. Kuo, S.-C. Hung, T.-S. Lee, D.-C. Tarng, Iron sucrose accelerates early atherogenesis by increasing superoxide production and upregulating adhesion molecules in CKD, J. Am. Soc. Nephrol. : JASN (J. Am. Soc. Nephrol.) 25 (11) (2014) 2596–2606, https://doi.org/10.1681/ASN.2013080838.

[20] S.P. Khadke, A.A. Kuvalekar, A.M. Harsulkar, N. Mantri, High energy intake induced overexpression of transcription factors and its regulatory genes involved in acceleration of hepatic lipogenesis: a rat model for type 2 diabetes, Biomedicines 7 (4) (2019) 76, https://doi.org/10.3390/biomedicines7040076.

[21] A. Fayi (Ed.), Expression of FABP6 and FABP9 in Prostate Cancer and Their Relationship to Malignant Progression, 2017.

[22] Matic L. Perisic, U. Rykaczewska, A. Razuvaev, M. Sabater-Lleal, M. Lengquist, Clint L. Miller, et al., Phenotypic modulation of smooth muscle cells in atherosclerosis is associated with downregulation of LMOD1, SYNPO2, PDLIM7, PLN, and SYNM, Arterioscler. Thromb. Vasc. Biol. 36 (9) (2016) 1947–1961, https://doi.org/10.1161/ATVBAHA.116.307893.

[23] Matic L. Perisic, U. Rykaczewska, A. Razuvaev, M. Sabater-Lleal, M. Lengquist, C.L. Miller, et al., Phenotypic modulation of smooth muscle cells in atherosclerosis is associated with downregulation of LMOD1, SYNPO2, PDLIM7, PLN, and SYNM, Arterioscler. Thromb. Vasc. Biol. 36 (9) (2016) 1947–1961, https://doi.org/10.1161/atvbaha.116.307893.

[24] M. Kurban, C.A. Kim, M. Kiuru, K. Fantauzzo, R. Cabral, O. Abbas, et al., Copy number variations on chromosome 4q26-27 are associated with Cantu syndrome, Dermatology (Basel, Switzerland) 223 (4) (2011) 316–320, https://doi.org/10.1159/000333800.

[25] J. Soh, J. Iqbal, J. Queiroz, C. Fernandez-Hernando, M.M. Hussain, MicroRNA-30c reduces hyperlipidemia and atherosclerosis in mice by decreasing lipid synthesis and lipoprotein secretion, Nat Med 19 (7) (2013) 892–900, https://doi.org/10.1038/nm.3200.

[26] H. Han, Y.-H. Wang, G.-J. Qu, T.-T. Sun, F.-Q. Li, W. Jiang, et al., Differentiated miRNA expression and validation of signaling pathways in apoE gene knockout mice by cross-verification microarray platform, Exp. Mol. Med. 45 (3) (2013) e13–e, https://doi.org/10.1038/emm.2013.31.

[27] S. Memczak, M. Jens, A. Elefsinioti, F. Torti, J. Krueger, A. Rybak, et al., Circular RNAs are a large class of animal RNAs with regulatory potency, Nature 495 (7441) (2013) 333–338, https://doi.org/10.1038/nature11928.

[28] T.B. Hansen, T.I. Jensen, B.H. Clausen, J.B. Bramsen, B. Finsen, C.K. Damgaard, et al., Natural RNA circles function as efficient microRNA sponges, Nature 495 (7441) (2013) 384–388, https://doi.org/10.1038/nature11993.

[29] T.B. Hansen, E.D. Wiklund, J.B. Bramsen, S.B. Villadsen, A.L. Statham, S.J. Clark, et al., miRNA-dependent gene silencing involving Ago2-mediated cleavage of a circular antisense RNA, EMBO J. 30 (21) (2011) 4414–4422, https://doi.org/10.1038/emboj.2011.359.

[30] P.-P. Guan, J.-W. Guo, X. Yu, Y. Wang, T. Wang, K. Konstantopoulos, et al., The role of cyclooxygenase-2, interleukin-1β and fibroblast growth factor-2 in the activation of matrix metalloproteinase-1 in sheared-chondrocytes and articular cartilage, Sci. Rep. 5 (2015) 10412, https://doi.org/10.1038/srep10412.

[31] E. Ricciotti, A. FitzGerald Garret, Prostaglandins and inflammation, Arterioscler. Thromb. Vasc. Biol. 31 (5) (2011) 986–1000, https://doi.org/10.1161/ATVBAHA.110.207449.

[32] F. Cipollone, M. Fazia, A. Iezzi, G. Ciabattoni, B. Pini, C. Cuccurullo, et al., Balance between PGD synthase and PGE synthase is a major determinant of atherosclerotic plaque instability in humans, Arterioscler. Thromb. Vasc. Biol. 24 (7) (2004) 1259–1265, https://doi.org/10.1161/01.ATV.0000133192.39901.be.

[33] H. Qiu, J.Y. Liu, D. Wei, N. Li, E.N. Yamoah, B.D. Hammock, et al., Cardiac-generated prostanoids mediate cardiac myocyte apoptosis after myocardial ischaemia, Cardiovasc. Res. 95 (3) (2012) 336–345, https://doi.org/10.1093/cvr/cvs191.

[34] K. Yuhki, F. Kojima, H. Kashiwagi, J. Kawabe, T. Fujino, S. Narumiya, et al., Roles of prostanoids in the pathogenesis of cardiovascular diseases: novel insights from knockout mouse studies, Pharmacol. Ther. 129 (2) (2011) 195–205, https://doi.org/10.1016/j.pharmthera.2010.09.004.

[35] R.C. Jin, B. Voetsch, J. Loscalzo, Endogenous mechanisms of inhibition of platelet function, Microcirculation 12 (3) (2005) 247–258, https://doi.org/10.1080/10739680590925493.

[36] Evaluation of colour pre-processing on patch-based classification of H&E-Stained images, in: F. Bianconi, J.N. Kather, C.C. Reyes-Aldasoro (Eds.), Digital Pathology, Springer International Publishing, Cham, 2019, 2019//.

[37] A. Blank, C. Schenker, H. Dawson, G. Beldi, I. Zlobec, A. Lugli, Evaluation of tumor budding in primary colorectal cancer and corresponding liver metastases based on H&E and pancytokeratin staining, Front. Med. 6 (2019) 247, https://doi.org/10.3389/fmed.2019.00247.

[38] S. Anders, Analysing RNA-Seq data with the DESeq package, Mol Biol 43 (4) (2010) 1–17.

[39] M. Kanehisa, M. Araki, S. Goto, M. Hattori, M. Hirakawa, M. Itoh, et al., KEGG for linking genomes to life and the environment, Nucleic Acids Res. 36 (suppl_1) (2007) D480–D484.

[40] M. Krzywinski, J. Schein, I. Birol, J. Connors, R. Gascoyne, D. Horsman, et al., Circos: an information aesthetic for comparative genomics, Genome Res. 19 (9) (2009) 1639–1645, https://doi.org/10.1101/gr.092759.109.

[41] L. Zhou, J. Chen, Z. Li, X. Li, X. Hu, Y. Huang, et al., Integrated profiling of microRNAs and mRNAs: microRNAs located on Xq27.3 associate with clear cell renal cell carcinoma, PLoS One 5 (12) (2010) e15224, https://doi.org/10.1371/journal.pone.0015224.
[42] C. Watanabe, Y. Seino, H. Miyahira, M. Yamamoto, A. Fukami, N. Ozaki, et al., Remodeling of hepatic metabolism and hyperaminoacidemia in mice deficient in proglucagon-derived peptides, Diabetes 61 (1) (2012) 74–84, https://doi.org/10.2337/db11-0739.
[43] Y.Y. Zhao, Y.L. Feng, X. Bai, X.J. Tan, R.C. Lin, Q. Mei, Ultra performance liquid chromatography-based metabonomic study of therapeutic effect of the surface layer of Poria cocos on adenine-induced chronic kidney disease provides new insight into anti-fibrosis mechanism, PLoS One 8 (3) (2013) e59617, https://doi.org/10.1371/journal.pone.0059617.